GPCR Antitarget Modeling: Pharmacophore Models for Biogenic Amine Binding GPCRs to Avoid GPCR-Mediated Side Effects**

Thomas Klabunde* and Andreas Evers[a]

G protein-coupled receptors (GPCRs) form a large protein family that plays an important role in many physiological and pathophysiological processes. However, the central role that the biogenic amine binding GPCRs and their ligands play in cell signaling poses a risk in new drug candidates that reveal side affinities towards these receptor sites. These candidates have the potential to interfere with the physiological signaling processes and to cause undesired effects in preclinical or clinical studies. Here, we present 3D cross-chemotype pharmacophore models for three biogenic amine antitargets: the α_{1A} adrenergic, the 5-HT$_{2A}$ serotonin, and the D2 dopamine receptors. These pharmacophores describe the key chemical features present within these biogenic amine antagonists and rationalize the biogenic amine side affinities found for numerous new drug candidates. First applications of the α_{1A} adrenergic receptor model reveal that these in silico tools can be used to guide the chemical optimization towards development candidates with fewer α_{1A}-mediated side effects (for example, orthostatic hypotension) and, thus, with an improved clinical safety profile.

Introduction

G protein-coupled receptors (GPCRs) form a large protein family that plays an important role in many physiological and pathophysiological processes. Historically, the discovery of drugs acting at GPCRs has been extremely successful with 50% of all recently launched drugs targeting GPCRs.[1] In particular, the subfamily of biogenic amine binding GPCRs has provided excellent drug targets (given in brackets) for the treatment of numerous diseases (Table 1), such as schizophrenia (mixed D2/D1/5-HT2 antagonists), psychosis (mixed D2/5-HT$_{2A}$ antagonists), depression (5-HT1 agonists), migraine (5-HT1 agonists), allergies (H1 antagonists), asthma (β2 agonists, M1 antagonists), ulcers (H2 antagoinst), and hypertension (α1 antagonist, β1 antagonist).

Table 1. *Biogenic amine binding GPCR targets, treated diseases, and drugs on the market.*

Target receptor (agonists/antagonists)	Disease	Generic name (Trademark)
histamine H1 (antagonists)	allergies	loratadine (Claritin), fexofenadine (Allegra/Telfast), Cetirizine (Zyrtec/Reactine)
histamine H2 (antagonists)	ulcers	raniditine (Zantac), Famotidine (Pepcidine/Gaster)
adrenergic β2 (agonists)	asthma	salmeterol (Serevent)
muscarinic M1 (antagonists)	asthma	ipratropium (Atrovent)
adrenergic α1 (antagonists)	hypertension	Doxazosin (Cardura)
adrenergic β1 (antagonists)	hypertension	metoprolol (Seloken)
serotonin 5-HT1 (agonists)	depression migraine	buspirone (Buspar) sumatriptan (Imigran/Imitex)
dopaminergic D2 and serotonin 5-HT2 (antagonists)	schizophrenia	olanzapine (Zyprexa)
dopaminergic D2 and serotonin 5-HT$_{2A}$ (antagonists)	psychosis	risperidone (Risperdal)

However, the central role that many of the biogenic amine binding GPCRs play in cell signaling also poses a risk in new drug candidates that reveal side affinities towards these receptor sites. These candidates have the potential to interfere with the physiological signaling processes and to cause undesired effects in preclinical or clinical studies. For example, the α_{1A} adrenergic receptor modulates the relaxation of the vascular muscle tone and is thus important for blood pressure regulation. It has been suggested as an antitarget that mediates cardiovascular side effects of many drug candidates, thereby causing orthostatic hypotension, dizziness, and fainting spells.[2,3] Furthermore, in order to obtain a clean clinical profile for novel development candidates, strong molecular interactions with dopamine and serotonin receptors (like the 5-HT$_{2A}$ and D2 receptors), which represent the molecular targets for many antipsychotics (for example, olanzapine or risperidone), need to be avoided.

In order to monitor affinity profiles of new drug candidates during compound optimization and to predict negative side effects during chemical optimization, Aventis has established biogenic amine receptor binding assays. Several lead compounds, not only targeting against biogenic amine receptors,

[a] *Dr. T. Klabunde, Dr. A. Evers*
Aventis Pharma Deutschland GmbH
A Company of the Sanofi–Aventis Group
Scientific and Medical Affairs, Drug Design, Industriepark Hoechst
Building G878, 65926 Frankfurt am Main (Germany)
Fax: (+49) 69-331-399
E-mail: thomas.klabunde@aventis.com

[**] *GPCR = G protein-coupled receptor.*

  DOI: 10.1002/cbic.200400369 *ChemBioChem* **2005**, *6*, 876 – 889

but also targeting against chemokine or peptide binding GPCRs, reveal affinities towards several members of the biogenic amine antitarget panel when they enter the chemical optimization phase. Reliable in silico tools to identify compounds with strong antitarget affinity and computational models to guide the chemical optimization towards compounds with a more favorable side-affinity profile are of great value for the design and development of new drug candidates.

In working towards this goal, we have generated pharmacophore models for GPCR antitargets. The challenge in the generation of these "cross-chemotype" pharmacophore models is the requirement that these models need to describe the receptor interaction points not only for a single chemical series but for several different compound classes. In addition, these pharmacophores need to capture sufficient pharmacophoric points to describe the important molecular interactions for the respective receptor. Here we report the generation and validation of 3D pharmacophore models rationalizing the affinity of several different chemical series for the α_{1A}, the 5-HT_{2A}, and the D2 receptors. First applications of the α_{1A} model within Aventis GPCR projects reveal that these models are capable of rationalizing the strong antitarget affinity of most lead series that reveal undesired side affinities and, thus, can guide the chemical optimization towards development candidates with a superior safety index.

Results and Discussion

Generation of antitarget pharmacophores

Selection of training sets: The training sets used for pharmacophore generation have been extracted from the Aureus database, a structure activity database for GPCR ligands compiled and maintained by Aureus Pharma.[4] The database covers all biological data published on GPCRs and provides chemical structure information, references to the original publication or patent, and detailed information on the experimental conditions (for example, the assay type, cell line, or radioligand used). We extracted only compounds that had been tested with identical experimental protocols for inhibition constant (K_i) determination in order to ensure the high quality and consistency of the training-set data. As functional data obtained from different laboratories and assay methods cannot be expected to provide comparable values, we used only biological data from radioligand displacement assays. In addition, only the most active compounds were considered within the training sets.

Adrenergic α_{1A} receptor antagonists with a K_i value of less than 100 nM when tested against the recombinant human wild-type receptor (as determined in a radioligand displacement assay by using the radioligand prazosin) were extracted from the Aureus database. The structure analysis of the compounds reveals that they can be grouped into two classes, probably binding to overlapping but not identical binding sites within the receptor. A similar classification of biogenic amine ligands has been proposed earlier by Jacoby et al.[5] We thus selected two diverse training sets covering chemotype examples of each class: class II antagonists are represented by 6 compounds revealing 2 aromatic rings and a positively ionizable group positioned 2–4 bond lengths from the aromatic features, while the 14 representatives of class I antagonists reveal a positively ionizable group which is separated from the first aromatic ring by 2–3 bond lengths and from the second aromatic ring by 6–7 bond lengths. Table 2 and Scheme 1 show the chemical structures of all training-set compounds, together with the reported binding affinities.

Serotonin 5-HT_{2A} receptor antagonists with a K_i value of less than 10 nM when tested against the recombinant human wild-type receptor (as determined in a radioligand displacement assay by using ketanserin as the radioligand) were extracted from the Aureus database. The structure analysis of the compounds reveals that they can be grouped into two classes. Accordingly, two diverse training sets covering chemotype examples of each class were selected: class I antagonists are represented by six compounds revealing two aromatic rings connected to polar hydrogen-bond donor and acceptor groups ("head" and "tail" groups) and a positive ionizable group positioned two to four bond lengths from the aromatic features, while the three representatives of class I antagonists reveal purely hydrophobic aromatic head groups. The chemical structures of all training-set compounds and the reported binding affinities are shown in Table 3 and Scheme 2.

Dopamine D2 receptor antagonists with a K_i value of less than 25 nM when tested against the recombinant human wild-type receptor (as determined in a radioligand displacement assay by using spiperone as the radioligand) were extracted

Table 2. *Training-set molecules for the α_{1A} adrenergic receptor and their affinity.*

Class	Compound	K_i [nM][a]
I	**1**	0.2
I	**2**	0.2
I	prazosin	0.3
I	NAN 190	0.4
I	RS 17053	0.5
I	**3**	0.5
I	doxazosin	0.8
I	**4**	1.0
I	**5**	2.8
I	**6**	4.6
I	cyclazosin	12.3
I	**7**	27.1
I	**8**	44
I	**9**	72.4
II	YM 617	0.04
II	WB 4104	0.1
II	ARC 239	0.4
II	BE 2254	0.4
II	spiperone	25.1
II	**10**	28.2

[a] K_i values are taken from the following references: **1** and **2**,[24] prazosin,[25] NAN 190, **6**, **7**, and **10**,[26] RS 17053 and YM617,[27] **3**, and **9**,[28] doxazosin, **5**, WB 4104, ARC 239, BE 2254,[29] **4**,[30] cyclazosin,[31] **8**,[32] and spiperone.[33]

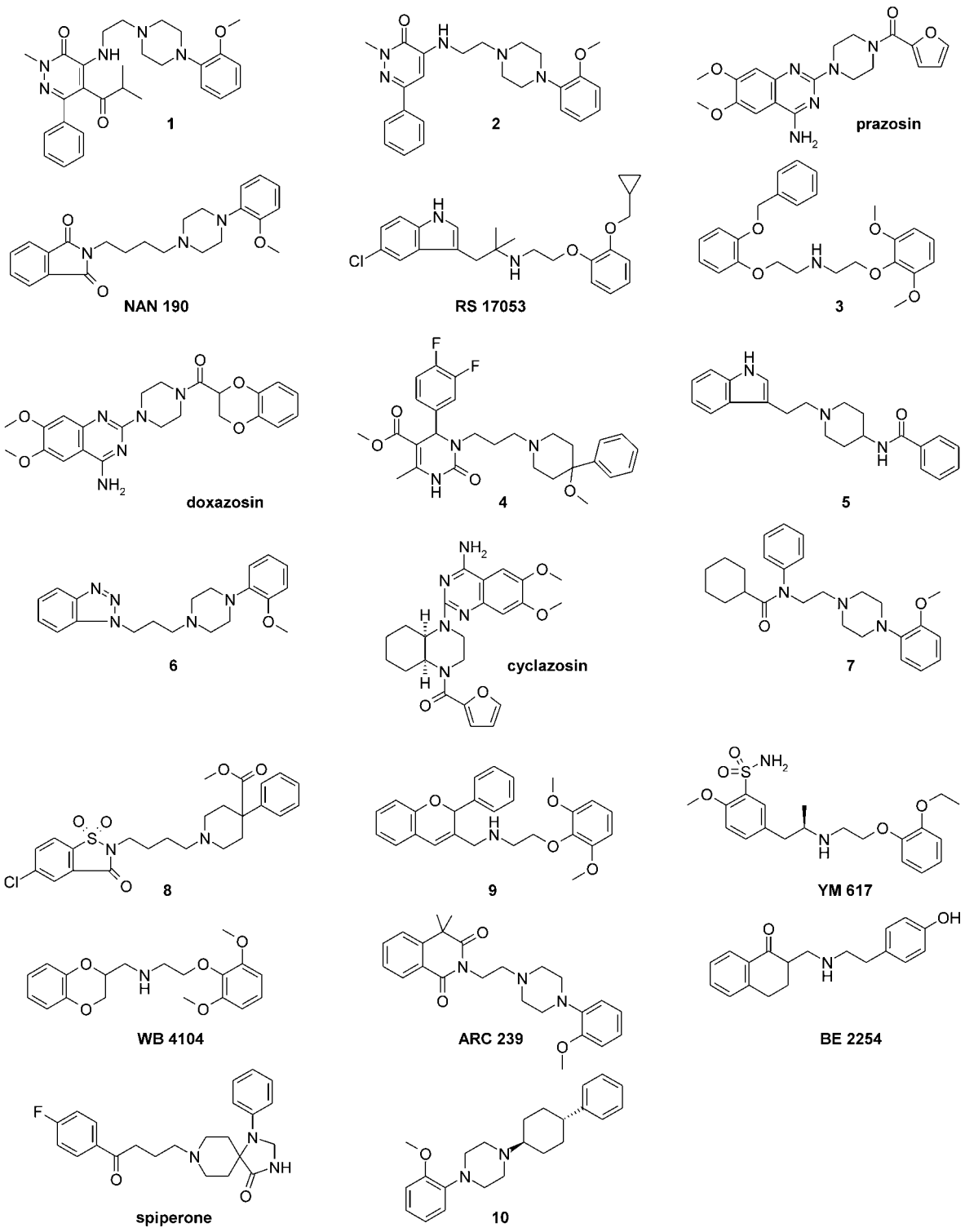

Scheme 1. *Adrenergic α_{1A} receptor anatagonists used as training-set compounds.*

from the Aureus database. The structure analysis of the compounds reveals that they can be grouped into two classes. We thus selected two diverse training sets covering chemotype examples of each class: class I antagonists are represented by four compounds revealing two aromatic rings connected to polar hydrogen-bond donor and acceptor groups (head and tail groups) and a positive ionizable group positioned two to four bond lengths from the aromatic features, while the six representatives of class II antagonists show purely hydrophobic aromatic head groups (similar to the 5-HT_{2A} class II antagonists). Table 4 and Scheme 3 reveal the chemical structures of all training-set compounds and the reported binding affinities.

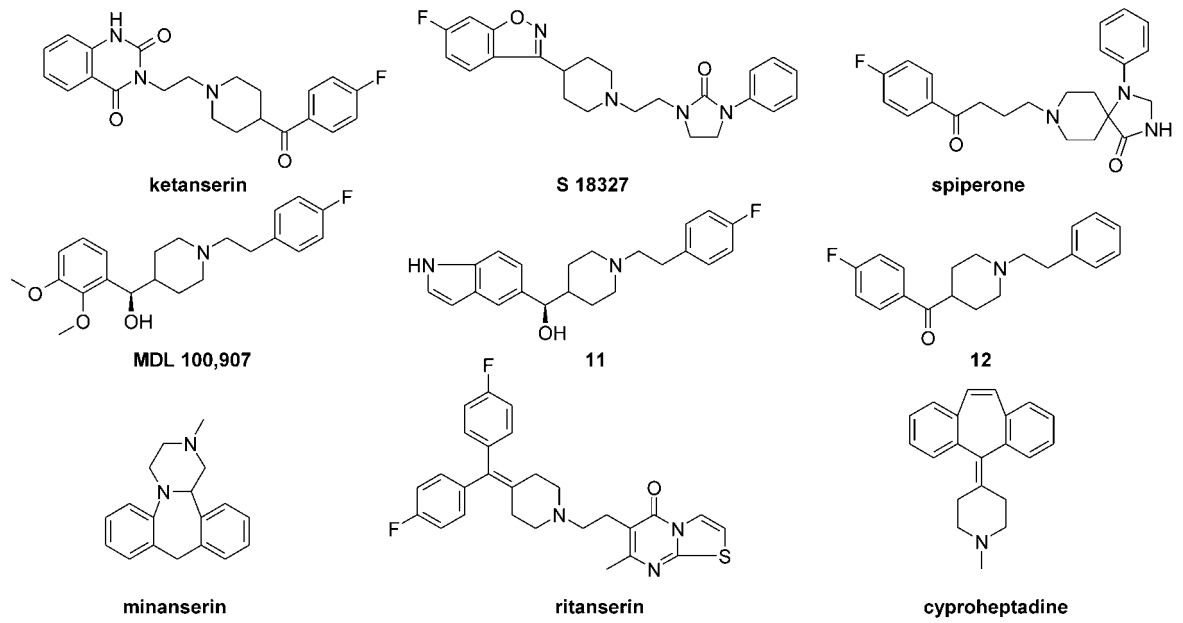

Scheme 2. *Serotonin 5-HT$_{2A}$ receptor anatagonists used as training-set compounds.*

Table 3. *Training-set molecules for the 5-HT$_{2A}$ receptor and their affinity.*

Class	Compound	K_i [nM][a]
I	ketanserin	0.9
I	S 18327	3.2
I	spiperone	1.0
I	MDL 100,907	0.8
I	**11**	14
I	**12**	4.9
II	minanserin	3.0
II	ritanserin	1.0
II	cyproheptadine	1.6

[a] K_i values are taken from the following references: ketanserin,[34] S 18327,[35] spiperone and ritanserin,[21] MDL 100,907, **11**, and **12**,[36] minanserin,[37] and cyproheptadine.[38]

Table 4. *Training-set molecules for the D2 receptor and their affinity.*

Class	Compound	K_i [nM][a]
I	spiperone	0.1
I	haloperidol	1.4
I	risperidone	2.3
I	domperidone	0.4
II	clozapine	28.0
II	chloropromazine	13.6
II	flupentixol	1.2
II	RMI 60947	21.0
II	loxapine	54.0
II	eticlopride	0.1

[a] K_i values are taken from the following references: spiperone, risperidone, and domperidone,[39] haloperidol,[40] clozapine,[41] chloropromazine,[42] flupentixol,[43] RMI 60947,[44] loxapine,[45] and eticolpride.[46]

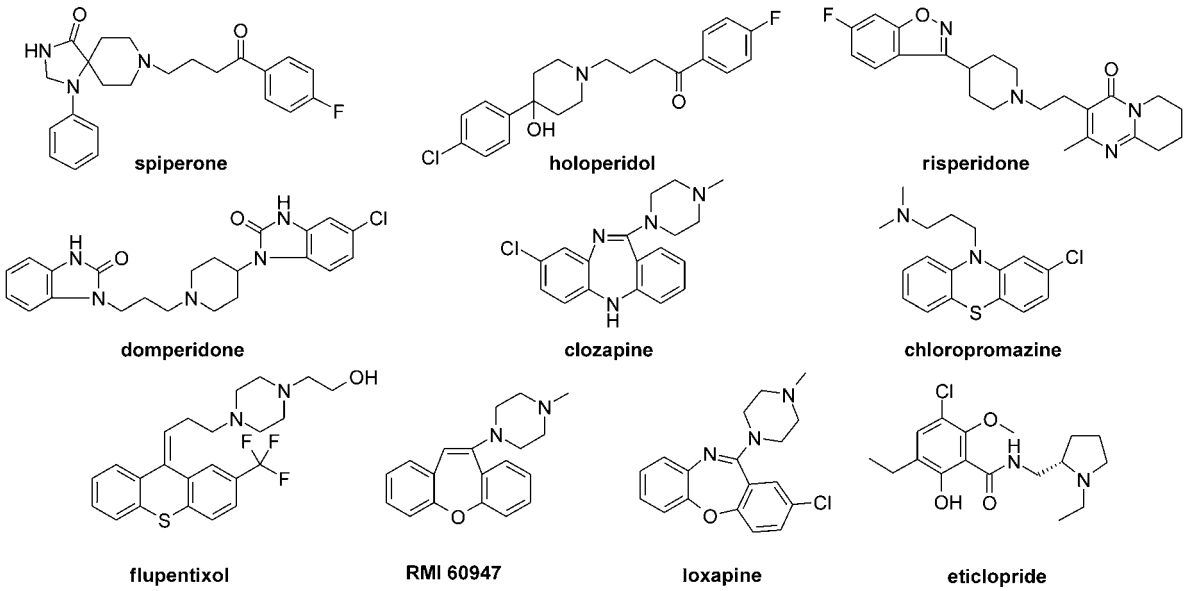

Scheme 3. *Dopaminergic D2 receptor anatagonists used as training-set compounds.*

Pharmacophore generation: The common-features hypothesis generation (Hiphop) module of Catalyst 4.7[6] was used for the generation of "cross-chemotype" 3D pharmacophores describing either the α_{1A}, the 5-HT_{2A}, or the D2 antagonists. The common-features hypothesis generation module is designed specifically for finding chemical features shared by a set of diverse compounds (different chemical classes) and for providing the relative alignments of the compounds, with the hypothesis expressing these common features (see the Experimental Section for details). For each training set, ten pharmacophore hypotheses were generated (three in the case of the 5-HT_{2A} class II training set). All hypotheses were visually inspected by mapping onto the training-set molecules. The major difference among the ten models (three in the case of the 5-HT_{2A} class II training set) generated from each training set was the mapping of the aromatic rings, either by the ring aromatic (RA) or by the hydrophobic (HY) functions. Only minor differences in the orientation of the RA vector were observed. Considering that all the generated pharmacophores map the training-set molecules in a similar way, the first model, the one ranked highest by the Catalyst scoring function (mapping all training-set molecules without partial matches if possible), was chosen for subsequent analysis and refinement in most cases. The pharmacophore features of the selected hypotheses are listed in Table 5. Only for the dopaminergic D2 class I training set was the first hypothesis not chosen; instead, the rank 4 hypothesis was chosen as it appeared superior due to an energetically more favorable conformation of spiperone mapping the hypothesis.

In order to improve the quality of the 3D pharmacophores, which means improving the quality of the generated relative compound alignments and the predictive power of the database searches, Catalyst allows the addition of spatial information. Based on the conformation of the respective lead ("principal") molecule mapping the 3D pharmacophore, a shape query was generated for each lead molecule and merged with the respective 3D pharmacophore.

Table 5. *Common-feature pharmacophore hypotheses generated for biogenic amine receptors.*

Receptor	Training set	N[a]	Selected hypothesis	Features[b]
adrenergic α_{1A}	class I	10	hypo 1	PI, HY, HY, HBA, HY (5)
	class II	10	hypo 1	PI, RA, HY, RA (4)
serotonin 5-HT_{2A}	class I	10	hypo 1	PI, HYA, HYA, HBA (4)
	class II	3	hypo 1	PI, RA, HY (3)
dopaminergic D2	class I	10	hypo 4	PI, RA, HY, HBA, HBA (5)
	class II	10	hypo 1	PI, RA, HY, HY (4)

[a] Number of hypotheses. [b] Abbreviations of features: HBA = hydrogen-bond acceptor, HY = hydrophobic, HYA = hydrophobic aromatic, PI = positively ionizable, RA = ring aromatic.

Description of GPCR antitarget pharmacophores

The common-feature pharmacophores (including the shape restraints) for the α_{1A}, 5-HT_{2A}, and D2 receptors derived from the training-set molecules (two sets for each receptor) are depicted in Figure 1 a–f. Two pharmacophores have been derived for each of the three biogenic amine receptors and these describe the key structural features required for the receptor binding seen in the structurally diverse antagonists of these receptors.

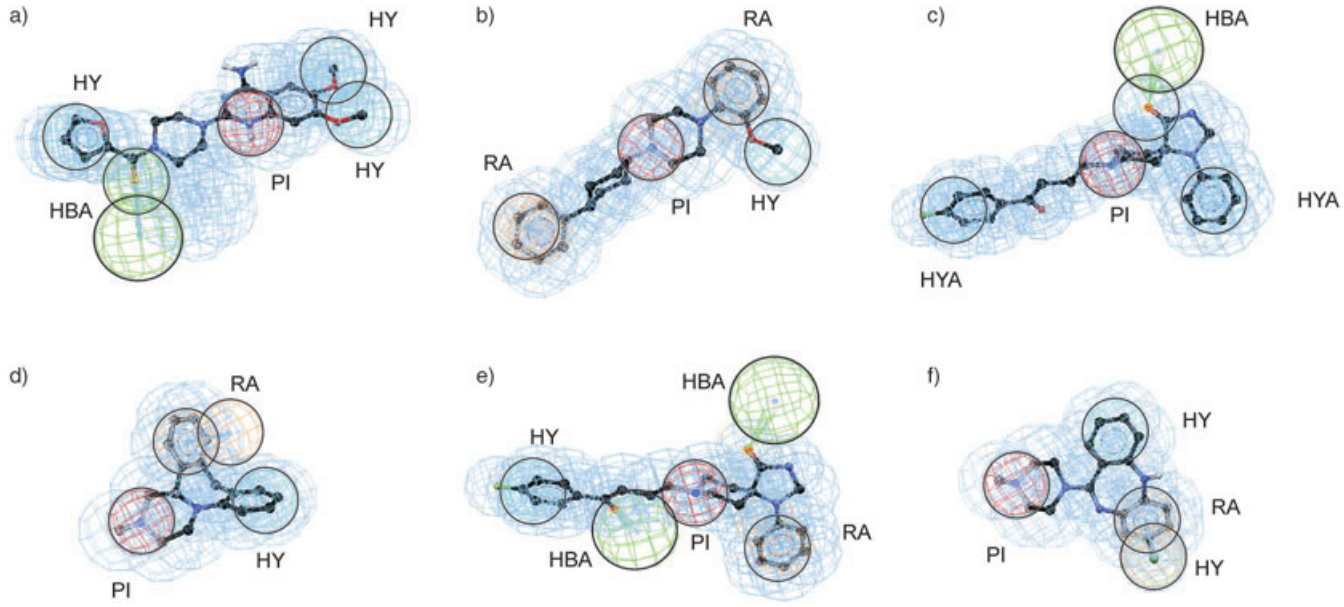

Figure 1. *Common-feature pharmacophores of three biogenic amine GPCR antitargets. A reference molecule from the training set has been mapped onto each pharmacophore. a) The adrenergic α_{1A} (class I) pharmacophore model is aligned to prazosin; B) the adrenergic α_{1A} (class II) pharmacophore model is aligned to compound* ***10****; C) the serotonin 5-HT_{2A} (class I) pharmacophore model is aligned to spiperone; D) the serotonin 5-HT_{2A} (class II) pharmacophore model is aligned to minanserin; E) the dopaminergic D2 (class I) pharmacophore model is aligned to spiperone; F) the dopaminergic D2 (class II) pharmacophore model is aligned to clozapine. The color scheme is red for positively ionizable (PI), green for hydrogen-bond acceptors (HBA), light blue for hydrophobic or hydrophobic aromatic (HY or HYA), and orange for ring aromatic (RA) pharmacophoric features. Shape restraints are shown in light blue.*

Adrenergic α_{1A} receptor pharmacophores: The two common-feature α_{1A} pharmacophores mapping the two different classes of high-affinity ligands of this adrenergic receptor subtype are shown in Figure 1a and b. The class I pharmacophore represents a five-point pharmacophore, which is composed of three hydrophobic moieties connected though a positively ionizable group (matched in Figure 1a by the N2 group of the quinazoline ring of the mapped compound prazosin) and a hydrogen-bond acceptor group (mapped by the amide group of prazosin). The class II pharmacophore describes the four main pharmacophoric points of the smaller class of α_{1A} ligands lacking the hydrogen-bond acceptor group but comprising two ring aromatic features, one hydrophobic moiety, and one positively ionizable feature (Figure 1b, mapping shown for **10**).

The similarity of the right-hand part of both pharmacophores (class I: positively ionizable, hydrophobic, hydrophobic; class II: positively ionizable, hydrophobic, ring aromatic) indicates that the head groups of class I and class II ligands mapping this part of the pharmacophore interact with the same site at the adrenergic receptor. However, the pharmacophores also reflect the differences among the two different types of α_{1A} receptor antagonists in the left-hand part. Class I ligands appear to share an acceptor group and a second hydrophobic group separated from the central positive charge by 9.5 Å (5–6 bond lengths). The shorter class II ligands, however, reveal an aromatic group connected by only 7.2 Å (2–4 bond lengths) to the positively charged nitrogen atom.

A pharmacophore model for the α_{1A} adrenergic receptor has also been described before by others.[7,8] Barbaro et al. used a series of pyridiazionone derivatives based on biological data from the rat receptor as a training set.[7] Their model resembles the class I pharmacophore described above in terms of pharmacophoric points and was shown to be well suited for a quantitative prediction of the biological activity of the training-set molecules and chemically closely related series. However, it does not represent a cross-chemotype model suitable for mapping a diverse set of different α_{1A} chemical compounds. The model generated by Bremner et al., on the other hand, was derived from a diverse set of 38 compounds.[8] However, it comprises only three pharmacophoric features and is thus quite generic and cannot be expected to be very selective.

Serotonin 5-HT$_{2A}$ receptor pharmacophores: The structural differences among 5-HT$_{2A}$ antagonists are more evident than those of the α_{1A} chemotypes (Scheme 2). Class I 5-HT$_{2A}$ antagonists are characterized by a positively ionizable group in the center of the molecule, a head group comprising an aromatic ring with polar functions, and a tail group containing an aromatic ring. Class II antagonists, on the other hand, share the positive charged nitrogen atom but also reveal a nonpolar hydrophobic head group, composed of two conformationally restricted aromatic rings. The tail function can be missing (for example, in minanserin) or present (for example, in ritanserin). The differences within the chemical structures are captured within the two pharmacophores generated for class I and class II 5-HT$_{2A}$ antagonists and shown in Figure 1c and d. The class I pharmacophore is made up of four pharmacophoric features (positively ionizable, two hydrophobic aromatic features, and a hydrogen-bond acceptor), which are mapped by all molecules of the training set. Spiperone is a subnanomolar D2 antagonist, which reveals significant affinity towards the 5-HT$_{2A}$ receptor ($K_i = 1$ nM) and has thus been included into the class I 5-HT$_{2A}$ training set. The mapping of spiperone onto the class I 5-HT$_{2A}$ pharmacophore is revealed in Figure 1c: the affinity of spiperone to the 5-HT$_{2A}$ receptor seems to be mediated mainly by the spiropiperidine moiety mapping three of the four pharmacophoric points and is supported by the aromatic ring of the butyrophenone tail. The class II pharmacophore on the other hand is formed by only three pharmacophoric points: a positively ionizable group, a ring aromatic feature, and a hydrophobic group (Figure 1d, mapping shown for minanserin). The pharmacophore reflects the chemical features of the class II antagonists mediating affinity towards the 5-HT$_{2A}$ receptor.

A comparison of the two pharmacophores suggests that both types of 5-HT$_{2A}$ receptor antagonists utilize similar interaction points at their receptor to harbor the positively ionizable group and a hydrophobic aromatic ring of the head group. For class II inhibitors these interaction points appear to be supplemented by an additional interaction of the other aromatic ring with the receptor. Class I inhibitors, in contrast, appear to address a hydrogen-bond donor in the receptor, thereby explaining the hydrogen-bond acceptor group found within these ligands. Moreover, they appear to have an additional interaction site within the receptor mediated by the hydrophobic aromatic feature in the tail group.

Dopaminergic D2 receptor pharmacophores: Like the 5-HT$_{2A}$ ligands, the antagonists of the dopaminergic D2 receptor can be classified into two groups (Scheme 3). Class I antagonists (for example, spiperone, haloperidol, risperidone, or domperidone) are characterized by a positively ionizable group in the center of the molecule, a head group comprising an aromatic ring with polar functions and an aromatic tail. Class II antagonists, on the other hand, lack the tail group and possess a head composed solely of aromatic and hydrophobic features. The two D2 pharmacophores are shown in Figure 1e and f, mapped onto one representative molecule of each training set. The class I five-point pharmacophore possesses positively ionizable, hydrophobic, ring aromatic, and two hydrogen-bond acceptor features. The class I D2 pharmacophore is thus very similar to the class I 5-HT$_{2A}$ pharmacophore. This is not a surprising finding as several biogenic amine ligands bind to both receptors with nanomolar affinity (for example, spiperone). In comparison to the 5-HT$_{2A}$ model, the D2 pharmacophore suggests one additional interaction point of the D2 ligands at the receptor mediated through the hydrogen-bond acceptor feature within the tail group. The similarity of the pharmacophores also indicates that the 5-HT$_{2A}$ and D2 receptor binding pockets harboring the class I 5-HT$_{2A}$ and D2 ligands have a high degree of similarity. The comparison suggests that the D2 receptor site might offer an additional hydrogen-bond donor group to bind the hydrogen-bond acceptor function found within the tail group of the D2 ligands.

The class II pharmacophore of the dopaminergic receptor is made up by four features: two hydrophobic groups, one aromatic ring, and one positively ionizable group. As for the class I model, similarities to the equivalent (class II) 5-HT_{2A} pharmacophore model are visible. The pharmacophores differ in that the D2 pharmacophore possesses one additional hydrophobic feature, which is present in most class II D2 antagonists (for example, chloro substituents seen for loxapine and eticlopride). The similarity of both pharmacophores again suggests a high degree of similarity of the 5-HT_{2A} and D2 receptor binding pockets addressed by the class II 5-HT_{2A} and the D2 ligands.

Validation of antitarget pharmacophores

The purpose of the common-feature antitarget pharmacophores is to recognize and rationalize antitarget side affinities within novel GPCR chemotypes different from those present in the Aurues training set. Therefore, it appears to be crucial to validate the pharmacophore hypotheses by using sets of external molecules not used for pharmacophore generation. Our aim was to verify that the pharmacophore is able to identify known α_{1A}, 5-HT_{2A}, and D2 antagonists and, thus, to verify the predictive ability of the pharmacophores. Towards this end, we performed a virtual screen of compound subsets extracted from the MDL Drug Data Report (MDDR; for details, see the Experimental Section):[9] 50 known α_{1A}, 5-HT_{2A}, and D2 inhibitors were extracted from the MDDR database and embedded into approximately 1000 MDDR molecules lacking the appropriate affinity (activity not stated in the MDDR database). The composition of each of the three test-set databases is shown in Table 6. To mark the predictive power of each pharmacophore, the hit rates (percentage of "true actives" in list of virtual hits) and yields (percentage of true actives identified by virtual screening) were calculated.

Table 6. *MDDR test-set databases used for pharmacophore validation.*

MDDR test set	Inactives[a]	Actives[a]
α_{1A}	998	50
5-HT_{2A}	979	50
D2	990	50

[a] Inactive and active compounds as stated within the MDDR database.

Adrenergic α_{1A} receptor pharmacophores: By virtual screening of the MDDR test set enriched with 50 α_{1A} ligands (Table 6) with the class I (class II) pharmacophore models, 82 (146) virtual hits were obtained for which 26 (42) are stated as α_{1A} antagonists (true actives). The hit rate was calculated as approximately 30% with both pharmacophores (see Table 7), which is 6 times higher than a random selection (4.8%). It is evident that the very restrictive class I 5-point pharmacophore misses approximately half of the 50 α_{1A} ligands embedded in the set (yield 52%). Thus, several series of α_{1A} antagonists present within the MDDR set do not belong to the class I α_{1A} receptor ligands. In contrast, the class II pharmacophore identifies most of the α_{1A} antagonists within the set (yield 84%) and reveals excellent specificity, reflected by a good hit rate. The virtual screening thus suggests that the less stringent class II four-point pharmacophore is especially suitable for recognizing most of the known α_{1A} antagonists and providing mappings of compounds with significant α_{1A} affinity. Taken together, both pharmacophores are able to identify 90% of the α_{1A} antagonists embedded into the test data set.

Table 7. *Hit rates and yields from screening the MDDR test-set database with the α_{1A}, 5-HT_{2A}, and D2 pharmacophores, respectively. The hit rate and yield are given for a virtual-screening protocol without considering the fit value of the virtual hits for ranking.*

	hits	No. of virtual true actives[a]	No. of identified	Hit rate[a]	Yield
α_{1A}	class I	82	26	32%	52%
	class II	146	42	29%	84%
	class I or II	168	45	27%	90%
5-HT_{2A}	class I	69	16	23%	32%
	class II	207	35	17%	70%
	class I or II	239	40	17%	80%
D2	class I	63	21	33%	42%
	class II	207	41	20%	82%
	class I or II	219	42	19%	84%

[a] Hit rate = (number of true actives in hit list)/(number of compounds in hit list) × 100; yield = (number of true actives in hit list)/(number of true actives in full database). The hit rate is calculated based on the assumption that all the compounds with MDDR-stated activity are active (true actives) and all the compounds with no stated activity against this target are inactive. However, it cannot be excluded that some of the inactive compounds identified by the pharmacophore hypothesis reveal actual activity on that target. The hit rate would thus be higher.

In many cases the performance of a pharmacophore-based virtual screen can be improved when the quality of the mapping to the respective pharmacophore is considered. Thus, we calculated the fit values of all test-set molecules onto both pharmacophores and ranked the virtual hits by the fit value of their mappings (see the Experimental Section). The resulting enrichment graphs are shown in Figure 2 for both pharmacophores. Both enrichment curves show a steep initial line running almost parallel to the ideal curve. The flattening of the curves towards the right-hand side can be explained by the fact that some α_{1A} database compounds cannot be mapped by the pharmacophore and thus obtain fit values of 0. The steepness of the enrichment curve on the left-hand side, however, reflects the fact that a high percentage of true α_{1A} ligands can be found among the top-ranked compounds of the database. (For example, among the top 10 scored virtual hits found by the class II pharmacophore, 6 are α_{1A} antagonists; this indicates a hit rate of 60% among the top 1% of the virtual hits.) Hit values, yield, and enrichment factor (found hit rate versus random hit rate) are listed in Table 8 for the top 5% scorers of both pharmacophores. Among the top 5% (52 highest ranked compounds) scorers of the database, 44% and 50% of the α_{1A} antagonists can be found by using the class I or class II pharmacophore as a filter, respectively. In addition to this excellent

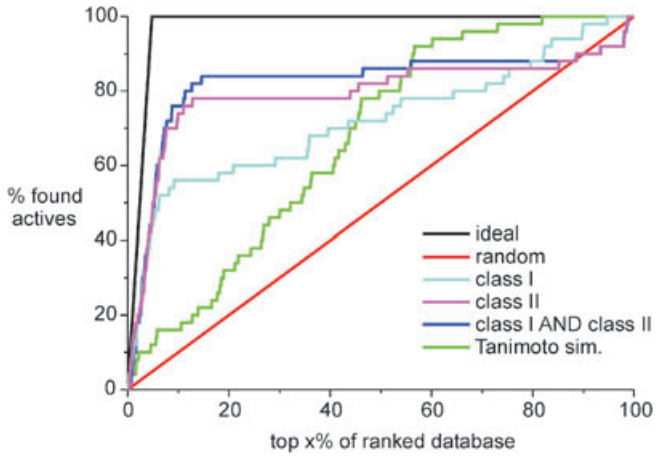

Figure 2. *Enrichment graph for virtual screening of 50 known α_{1A} antagonists embedded in the 1048 compound random MDDR library. The curve shows the relative ranking of the known antagonists. Database compounds are ranked along the x axis based on the fit value. The hit rate obtained by the class II pharmacophore (magenta) at a yield of 50% is tenfold better than random selection.*

Table 8. *Hit rate, yield, and enrichment factors for the top 5% scorers from screening the MDDR test-set database with the α_{1A}, 5-HT$_{2A}$, and D2 pharmacophores, respectively. All compounds have been scored based on their fit value on the respective pharmacophore.*

		No. of true actives among the top 5% of database[a]	Hit rate[a]	Yield	Enrichment factor
α_{1A}	class I	22	42%	44%	8.8
	class II	25	48%	50%	10
5-HT$_{2A}$	class I	14	27%	28%	5.7
	class II	13	25%	26%	5.3
	class I + II	21	41%	42%	8.5
D2	class I	20	39%	40%	8.1
	class II	10	20%	20%	4.2
	class I + II	12	24%	24%	5
all	random	2.5	4.8%	5%	1
	ideal	50	98%	100%	20

[a] Hit rate and yield are defined in the footnote of Table 7. The hit rate is calculated based on the same assumptions as those given in the footnote of Table 7. It is therefore possible that the hit rate and enrichment factor are actually higher.

yield, enrichment factors of approximately nine and ten, respectively, can be obtained by the pharmacophores when the hit rate of the pharmacophore-based selection is compared to a random selection. The hit rate is calculated based on the assumptions that all compounds with α_{1A} activity reported in the MDDR are active and that compounds with no α_{1A} activity reported in the MDDR against this target are inactive. However, the possibility cannot be excluded that some of the stated inactive compounds identified by the pharmacophore hypothesis reveal activity on the α_{1A} receptor. Among the top ten scored virtual hits, six are stated α_{1A} antagonists. The remaining four compounds have stated activity against serotonin receptors. Thus, a (cross-)activity towards the α_{1A} receptor is likely, which suggests even higher hit rates and yields than calculated.

At this point, it should also be noted that the excellent hit rate and yield generated, by the class II pharmacophore especially, cannot be explained by the structural similarity of MDDR test-set molecules to the Aureus training-set molecules. Tanimoto distances from the 50 α_{1A} antagonists within the MDDR test-set molecules have been calculated to all 6 molecules from the Aureus training data set (see the Experimental Section). Only 2 MDDR α_{1A} antagonists reveal a similarity of >0.8, for another 6 the Tanimoto distance is between 0.5 and 0.8, and for the remaining 42 a similarity of <0.5 is calculated (based on Unity fingerprints). Figure 2 reveals that the yield and hit rate generated by ranking the database compounds based on their maximal Tanimoto similarity (green curve) to the six reference molecules is not significantly higher than a random selection.

The excellent performance in terms of yield and enrichment factor of both pharmacophores suggests that both pharmacophores can also be useful filters for virtual screening to identify α_{1A} antagonists within large compound repositories. Indeed, both pharmacophores have been successfully applied at Aventis in a virtual-screening approach combining pharmacophore-based and homology-model-based virtual screening.[10] By using this approach, novel α_{1A} antagonists with nanomolar affinity could be identified from the company's compound collection.

Serotonin 5-HT$_{2A}$ receptor pharmacophores: The virtual screening of the MDDR test set enriched with 50 5-HT$_{2A}$ ligands (Table 6) with the 4-point class I pharmacophore and with the more generic 3-point pharmacophore for class II ligands provided 69 (class I) and 207 (class II) virtual hits. Within the list of these virtual hits, 16 (class I) and 35 (class II) 5-HT$_{2A}$ antagonists were covered, thereby giving hit rates of 23 and 17%, respectively (see Table 7). It is evident that the class I four-point pharmacophore is able to recognize most of the class I 5-HT$_{2A}$ antagonists and is also selective in terms of not mapping too many MDDR entries with no stated 5-HT$_{2A}$ affinity (hit rate 23%). However, it fails to recognize the structurally different class II 5-HT$_{2A}$ antagonists, which are frequently represented within the MDDR test set. The class II pharmacophore, on the other hand, identifies many of the 5-HT$_{2A}$ antagonists within the MDDR test set (yield 70%) but lacks the good selectivity (hit rate 17%). Taken together, both cross-chemotype pharmacophores identify 80% of all stated 5-HT$_{2A}$ antagonists within the MDDR test set.

As with the α_{1A} pharmacophores, we attempted to improve the hit rate and yield of the virtual screens by considering the fit value of their mappings. For both virtual screens, the fit values of the mappings of the virtual hits were calculated and the data base compounds were ranked according to their individual fit values as well as based on the sum of the fit values found for the mapping on either pharmacophore. The enrichment plots are shown in Figure 3. As seen for the α_{1A} pharmacophores, both enrichment curves show a steep beginning, which reflects the fact that a high percentage of true 5-HT$_{2A}$ li-

gands can be found among the top-ranked compounds of the database (top 1–10%). Again, a flattening of the curves is seen, at 6% (class I) or 14% (class II) on the *x* axis, because not all 5-HT_{2A} inhibitors embedded in the data set can be mapped. A consensus ranking based on the sum of the fit values ob-

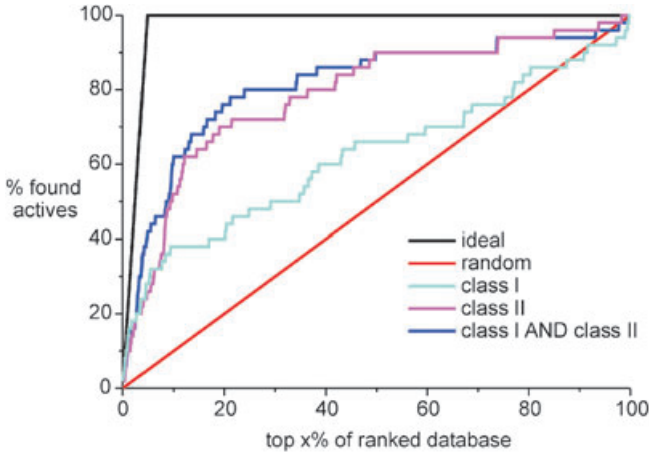

Figure 3. *Enrichment graph for virtual screening of 50 known 5-HT_{2A} antagonists embedded in the 1029 compound random MDDR library. The curve shows the relative ranking of the known antagonists. Database compounds are ranked along the* x *axis based on the fit value. The hit rate obtained by the sum of the class I and class II pharmacophore at a yield of 50% is eightfold better than random selection.*

tained for the mappings on both pharmacophores (blue curve) appears to provide the best results. Hit values, yield, and enrichment factor are listed in Table 8 for the top 5% scorers obtained. The values show that, among the top 5% virtual hits scored by the class I and class II pharmacophores, 42% of all embedded 5-HT_{2A} antagonists are found and hit rates 8.5 times higher than those with a random selection can be obtained. The virtual screening of the MDDR data set reveals that the 5-HT_{2A} pharmacophores appear to be suitable for recognizing most 5-HT_{2A} antagonists and for providing pharmacophore mappings of compounds with significant 5-HT_{2A} affinity.

Dopaminergic D2 receptor pharmacophores: The virtual screening of the MDDR test set enriched with 50 D2 ligands (Table 6) with the 5-point class I pharmacophore and with the more generic 4-point pharmacophore for class II ligands provided 63 (class I) and 207 (class II) virtual hits. Within the list of these virtual hits, 21 (class I) and 41 (class II) D2 antagonists were covered, thereby givng hit rates of 33% and 20%, respectively (versus a hit rate of 5% for random selection; Table 7). It is evident that the class I five-point pharmacophore is able to recognize most of the class I D2 antagonists and is also selective in terms of not mapping too many MDDR entries with no stated D2 affinity (hit rate 33%). However, it fails to recognize the structurally different class II D2 antagonists, which are frequently represented within the MDDR test set; this explains the yield of just 42%. The class II pharmacophore, on the other hand, identifies many D2 antagonists within the MDDR test set (yield 82%) but lacks the selectivity, in that it also maps 166 compounds within the database that do not have explicitly stated D2 antagonism.

As with the α_{1A} pharmacophores, we attempted to improve the hit rate and yield of the virtual screens by considering the fit value of their mappings. For both virtual screens, the fit value of the mappings of the virtual hits were calculated and the data base compounds were ranked according to their individual fit values as well as based on the sum of the fit values found for the mapping on either pharmacophore. Table 8 summarizes hit rates and yields for the top 5% scorers. The table reveals that the hit rate of the class I D2 pharmacophore could be slightly improved when the fit value is considered for the ranking of the virtual hits.

Guidance of chemical optimization to improve side-affinity profiles

In order to monitor affinity profiles of novel drug candidates during compound optimization, as well as of compounds within GPCR-hit-finding libraries, Aventis has established a panel of biogenic amine receptor binding assays. Up to now, several hundred compounds coming from GPCR-directed libraries or originating from Aventis drug-discovery programs have been profiled against the Aventis biogenic amine antitarget panel. Table 9 lists the relative frequency of observed side affinities. The experimental data reveal that approximately 14% of the profiled compounds have moderate ($IC_{50} < 1$ μM) α_{1A} affinity in the submicromolar range. The frequency of observed moderate ($IC_{50} < 1$ μM) 5-HT_{2A} affinity is 9%. 3.5% of all tested

Table 9. *Relative frequency of IC_{50} values observed against GPCR antitargets.*

	$IC_{50} < 100$ nM	$IC_{50} < 1$ μM
α_{1A}	3.5%	14%
5-HT_{2A}	3.5%	9%
D2	0%	0.6%

compounds reveal strong α_{1A} binding with affinities of less than 100 nM. Strong 5-HT_{2A} affinity is seen with the same frequency. These experimental results reveal the need for optimization of the side-affinity profile of several compounds for the further development of these drug candidates.

The main application of the generated common-feature antitarget pharmacophore hypotheses is the recognition of antitarget side affinities within novel chemotypes. The aim is to use the pharmacophores to rationalize the experimental findings by providing the pharmacophore mappings. Recognition of the key chemical features that are responsible for the side affinities could then provide guidance for the chemical optimization of these series towards compounds with a more favorable side-affinity profile.

80% of all experimentally identified α_{1A} binders could be mapped onto the class II α_{1A} pharmacophore (for details, see the Experimental Section) fulfilling all four pharmacophore points and the generated shape requirement. (Only 50% of

the weak binders could be mapped without allowing partial matches, a result indicating that approximately half of the weaker compounds lack at least one pharmacophoric point of the four-point pharmacophore.) Mapping of one of these compounds onto the α_{1A} class II pharmacophore is shown in Figure 4. The mapping directly indicates the chemical features

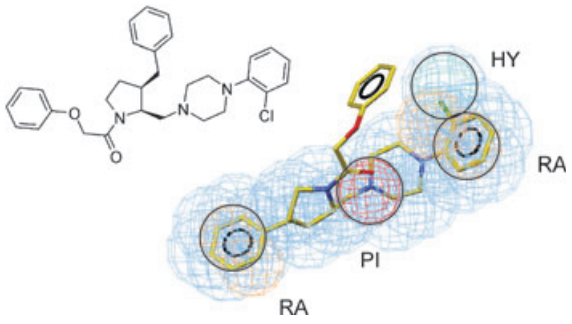

Figure 4. *Pharmacophore mapping of a high-affinity α_{1A} binder identified within the Aventis antitarget panel mapped onto adrenergic α_{1A} (class II) pharmacophore model. All pharmacophoric points are mapped. The alignment suggests that removal of the chlorine substituent from the 4-phenylpiperidine will reduce the unfavorable side affinity for the α_{1A} receptor.*

that are mediating the strong affinity towards this subtype of the adrenergic receptor: These are the positive charge of the piperazine moiety, the *ortho*-substituted phenyl ring on position 4 of the piperazine, and the aromatic ring of the benzyl chain. The mapping onto the class II pharmacophore thus provides direct guidance for the chemical optimization of the respective series to avoid the undesired α_{1A} affinity (for example, removal of the chlorine substituent within the 4-phenyl piperazine).

Mapping of pharmacophore models into receptor sites

Numerous site-directed mutagenesis studies have provided a conclusive picture for molecular interactions between the receptor-activating biogenic amines (for example, serotonin, epinephrine, dopamine) and their respective receptors:[11–15] a highly conserved aspartate residue in transmembrane helix TM3 (Asp3.32 according to the Ballesteros–Weinstein nomenclature), conserved serine residues in TM5 (for example, Ser5.42 and Ser5.46 for α_{1A}), and hydrophobic phenylalanine residues from TM6 have been identified to be important for agonist binding. In addition, through mutational studies and comparative affinity determinations based on ligand binding, the essential amino acids involved in antagonist recognition have been identified for the α_{1A},[15–17] 5-HT_{2A}[18,19] and D2 receptors.[14,19] According to these studies, the binding pocket of the prototype biogenic amine receptor antagonist stretches from the agonist binding site formed by TM3, TM5, and TM6—interacting with the antagonist's head group—towards the transmembrane helices TM1, TM2, and TM7, which have been suggested to harbor the lipophilic tail moiety of several antagonists.

Based on these experimental data, topographical interaction models for all three biogenic amine receptors have been generated (Figure 5). The generated pharmacophore models have been mapped into the topographical interaction models to suggest the putative interaction points of each pharmacophoric feature with its receptor:

1) The positive ionizable pharmacophoric feature is thought to be anchored through a salt bridge to the conserved aspartate residue in TM3.
2) The hydrophobic and aromatic features of the head moieties are harbored within hydrophobic microdomains formed by aromatic and aliphatic side chains of TM4, TM5, and TM6. The "floor" of this hydrophobic microdomain is formed by several conserved aromatic amino acids (Phe6.44, Trp6.48, Phe5.47), which are conserved among the family of biogenic amine GPCRs, a fact also explaining the similarity of the pharmacophoric features.
3) The polar residue at position 6.55 (asparagine in 5-HT_{2A}, histidine in D2) might address the hydrogen-bond acceptor group found within many class I 5-HT_{2A} and class I D2 ligands (Figure 5c, e). In contrast, within the α_{1A} receptor the residue 6.55 is a methionine; this provides a possible explanation for the fact that in this receptor only hydrophobic (aromatic) pharmacophoric features appear to be essential for strong α_{1A} binding.
4) The hydrophobic or ring aromatic feature observed within the tail moiety of almost all α_{1A} antagonists, as well as within class I 5-HT_{2A} and class I D2 ligands, is likely to be directed towards aromatic and hydrophobic residues within helices TM3 (3.28) and TM2 (2.64; Figure 5a–c, e).
5) A threonine residue in position 7.39 could act as a hydrogen-bond donor to the hydrogen-bond acceptor feature seen within the class I D2 pharmacophore (Figure 5e). A possible interaction partner for the hydrogen-bond acceptor within the α_{1A} class I pharmacophore could be Lys7.36 (not shown). However, this possiblity still needs to be validated by experimental mutagenesis data.
6) Less is known about the interaction sites for class II 5-HT_{2A} and D2 antagonists, which lack the hydrophobic tail moiety seen in class I antagonists. Comparison of the pharmacophores indicates that the class II antagonists bind into the agonist binding site (located between TM3, TM5, and TM6) as depicted in Figure 5d, f.

Conclusion

In conclusion, we present 3D "cross-chemotype" pharmacophore models for the α_{1A}, the 5-HT_{2A}, and the D2 receptors. Two pharmacophore models have been generated for each receptor to cover the main structural classes of α_{1A}, 5-HT_{2A}, and D2 antagonists. The pharmacophores have been generated from diverse training sets and describe the key pharmacophoric features present within these biogenic amine antagonists. All six pharmacophore models presented here offer acceptable levels of predictivity as revealed by virtual screening of MDDR

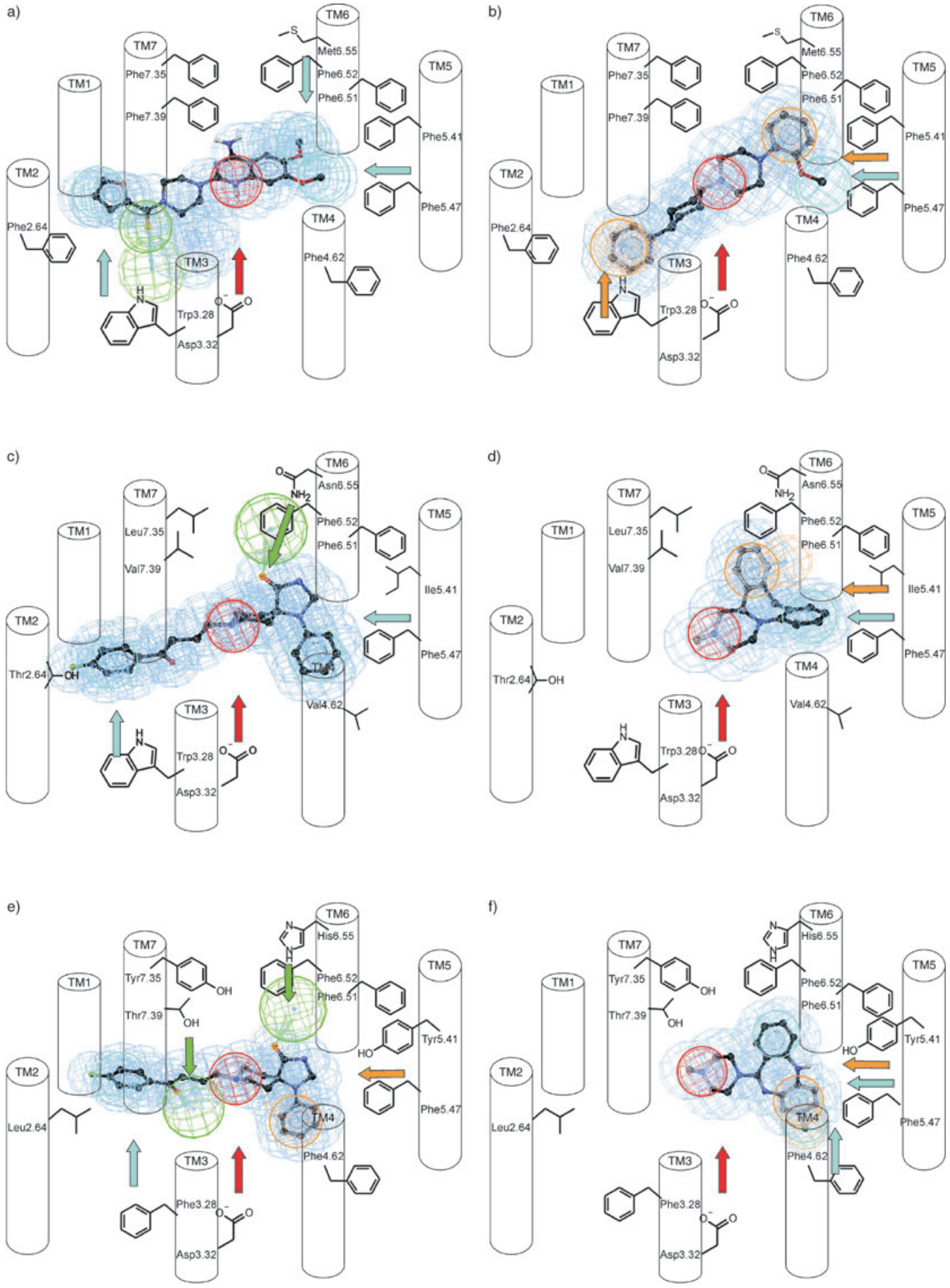

test sets, from which the models retrieved embedded antagonists with good yields and enrichment factors. The validation made on ligands taken from the MDDR database reveals that the models are indeed predictive for compounds different from those used for pharmacophore generation and that they recognize most structural classes of α_{1A}, 5-HT_{2A}, and D2 antagonists. Application of the α_{1A} model in a virtual screening approach in fact shows that the pharmacophores can be useful filters to identify α_{1A} antagonists within large compound repositories. A combination of a pharmacophore-based search with homology-model-based virtual screening provided novel α_{1A} antagonists with nanomolar affinity from the company's compound collection.[10]

Most important, however, is the application of these pharmacophore models in understanding the side affinities for biogenic amine receptors found for numerous new GPCR drug candidates. The pharmacophore model was able to identify 80% of the strong α_{1A} binders (IC_{50} value in radioligand displacement <100 nM) coming from Aventis (GPCR) projects and GPCR-targeted libraries, thereby allowing the recognition of the key chemical features that mediate this side affinity within these series. First applications of the α_{1A} adrenergic model reveal that these in silico tools can be used to guide the chemical optimization towards clinical candidates with fewer α_{1A}-mediated side effects (orthostatic hypotension, dizziness, fainting spells). All the presented models may be used in conjunction with existing in vitro methods to avoid undesired side affinities on these GPCR antitargets and to support the discovery of GPCR drugs with favorable clinical safety profiles.

Experimental Section

Pharmacophore generation: The chemical structures of all compounds in the training set were imported directly from the Aureus database (by using the sd file format). The molecules were manually inspected to ensure that no corrupted chemical structures were imported. In order to reflect the correct protonation state,[7] the N2 atom of the quinazoline ring of prazosin derivatives in the α_{1A} training sets was manually protonated by using the 2D and 3D sketcher of Catalyst;[6] this was necessary to allow Catalyst to recognize the N2 nitrogen atom as the positively ionizable group during pharmacophore generation. A conformational set was generated for each molecule by using the poling algorithm and the "best-quality conformational analysis" method, based on the CHARMm force field (Catalyst catConf module). All conformers within 20 kcal mol^{-1} in energy from the global minimum were considered for the pharmacophore generation. For each data set, one molecule (a representative of the class with good affinity and a small number of conformers) was chosen as the principal molecule (adrenergic α_{1A} (class I): prazosin; adrenergic α_{1A} (class II): compound **10**; serotonin 5-HT_{2A} (class I): spiperone; serotonin 5-HT_{2A} (class II): minanserin; dopaminergic D2 (class I): spiperone; dopaminergic D2 (class II): clozapine). For the principal molecule, all of its chemical features are considered in building hypothesis space. For all other molecules within the training set, a principal value of one was chosen and the "MaxOmitFeat" column was set to one, thereby allowing only hypotheses with features that are mapped completely by all compounds of the training set or hypotheses for which only one pharmacophoric feature is missed by a training-set molecule. The following features, included in Catalyst's features dictionary, were considered for the generation of common-feature hypothesis: positively ionizable (PI), hydrophobic (HY), hydrophobic aromatic (HYA), ring aromatic (RA), hydrogen-bond donor (HBD), and hydrogen-bond acceptor (HBA). In order to improve the quality of the 3D pharmacophores, Catalyst allows the addition of spatial information. Based on the conformation of the respective lead (principal) molecule mapping the 3D pharmacophore, a shape query was generated for each lead molecule and merged with the respective 3D pharmacophore. The tolerances for the shape queries (box volume match and similarity tolerance) were chosen in such a way that the mapping of the test-set molecules was not restricted by the presence of the shape restraint (similarity tolerance: 40%; box volume match: 70–130% for class I models, 50–150% for class II models).

Figure 5. *Topographical interaction models generated based on public site-directed mutagenesis data for the three biogenic amine receptors. Pharmacophore models (see Figure 1) have been mapped into the respective topographical receptor model. The models reveal putative receptor interaction sites for most of the pharmacophoric features observed within each antagonist class. A) α_{1A} (class I) pharmacophore and receptor model; the reference compound is prazosin; B) α_{1A} (class II) pharmacophore and receptor model; the reference compound is compound* ***10****; C) 5-HT_{2A} (class I) pharmacophore and receptor model; the reference compound is spiperone; D) 5-HT_{2A} (class II) pharmacophore and receptor model; the reference compound is minanserin; E) D2 (class I) pharmacophore and receptor model; the reference compound is spiperone; F) D2 (class II) pharmacophore and receptor model; the reference compound is clozapine. The color scheme for the pharmacophoric features is the same as that in Figure 1. Arrows indicate putative molecular interactions between the pharmacophoric points and the receptor sites. The arrow color code indicates the type of molecular interaction: light blue: hydrophobic; red: salt bridge to negative ionizable group from receptor (Asp3.32), green: hydrogen-bonding to receptor donor site (for example, His6.55 or Asn6.55); orange: aromatic stacking interaction.*

Generation of MDDR test-set database and virtual screening: The MDDR is an annotated database covering the patent literature, journals, meetings, and congresses and containing over 141 000 biologically relevant compounds and well-defined derivatives such as drugs launched or under development. To make the test sets, the MDDR database was filtered for α_{1A}, 5-HT_{2A}, and D2 antagonists and three compound sets were generated containing MDDR molecules enriched with α_{1A}, 5-HT_{2A}, and D2 antagonists. It should be noted that compounds could reveal affinity against one of these antitargets even though no activity is explicitly stated within the MDDR. The content of each database set is reflected in Table 6. The three subsets were converted for Catalyst by using the catConf option. In order to reflect the correct protonation state,[7] the N2 atom of the quinazoline ring of prazosin derivatives in the α_{1A} test sets was manually protonated by using the 2D and 3D sketcher of Catalyst. For each molecule, a conformational set within 20 kcal mol^{-1} of energy from the global minimum was generated. The databases were virtually screened by using the two respective 3D pharmacophore hypotheses (class I and class II) with the citest option within Catalyst. Only those compounds mapping all pharmacophoric features were retrieved as virtual hits (omit parameter set to zero). In order to evaluate the performance of the virtual screen, two properties of each generated virtual hit list were computed: the hit rate and the yield. The hit rate describes the percentage of true actives in the list of virtual hits (hit rate = number of true actives in hit list/number of compounds in hit list $\times$ 100). A random screening of the full database of 50 active compounds embedded into a set of approximately 1000 molecules would thus provide a hit rate of approximately 5%. The yield is defined as the percentage of true actives of all active compounds within the data-

base retrieved by virtual screening (yield = number of true actives in hit list/number of true actives in full database). In order to prioritize the virtual hits, fit values were extracted from the citest output file to reflect the quality of the mapping onto the pharmacophore for each compound. The fit values were used for the ranking of the virtual hits and the calculation of enrichment plots (yield as a function of the percentage of the database evaluated ranked by fit value).

Similarities of Aureus training sets and MDDR test sets: To check if the success in the predictivity of the pharmacophores is due to the fact that the compounds of the MDDR test set reveal structural similarity to the molecules of the training set, the similarity of the MDDR test-set molecules to all the molecules of the training set was calculated by using Tanimoto coefficients (based on Unity fingerprints) in the SYBYL program.[20] Tanimoto coefficients are defined as $N_{AB}/(N_A+N_B-N_{AB})$, where N_A and N_B are the number of bit sets on (that is, 1) in bit strings (binary representation of molecular structure) for molecules A and B, respectively, and N_{AB} is the number of bits that are common to both. The value of the Tanimoto coefficient varies between 0 and 1. The lower the coefficient, the smaller is the similarity between the molecules being compared.

Generation of Aventis test database and virtual screening: In order to check if the α_{1A} pharmacophore models are able to provide mappings of the strong α_{1A} binders as identified from the biogenic amine radioligand assay panel, the molecular structures were converted from an sd file for Catalyst by using the catConf option; for each molecule, a conformational set within 20 kcal mol^{-1} of energy from the global minimum was generated. The database was virtually screened by using the two respective pharmacophore hypotheses (class I and class II) with the citest command within Catalyst. Compounds mapping all pharmacophoric features were retrieved as virtual hits (omit parameter set to zero) and the pharmacophore alignments allowing the best fit were saved.

Experimental testing: D2, α_{1A}, and 5-HT$_{2A}$ receptor binding assays were performed as described elsewhere.[21–23] Briefly, for the D2 receptor, the binding of 1.5 nM [^{3}H]-spiperone (supplier NEN) to human recombinant D2 receptor in CHO-K1 cell membranes (4 μg per well) was measured after incubation for 30 min at 37 °C in 25 mM 2-[4-(2-hydroxyethyl)-1-piperazinyl)]ethanesulfonic acid (HEPES; pH 7.4, 200 μL) containing 5 mM $MgCl_2$, 1 mM $CaCl_2$, and 0.5 % bovine serum albumin (BSA). For the α_{1A} receptor radioligand displacement assay, 0.5 nM [^{3}H]-prazosine (supplier NEN) was used as the radioligand. Recombinant adrenergic α_{1A} receptor in CHO-K1 cell membranes (30.4 μg per well) was incubated for 40 min at 37 °C in 50 mM tris(hydroxymethyl)aminomethane/HCl (Tris/HCl; pH 7.7, 200 μL). For the 5-HT$_{2A}$ receptor, the binding of 1 nM [^{3}H]-ketanserine (supplier NEN) to human recombinant 5-HT$_{2A}$ receptors in CHO-K1 cell membranes (15 μg per well) was measured after incubation for 15 min at 37 °C in 50 mM Tris/HCl (pH 7.4, 200 μL). For all three assays, binding reactions were terminated by filtration through Millipore GF/B filter plates and radioactivity was determined with a liquid scintillation counter (Perkin–Elmer). IC_{50} values were calculated from the averages of double determinations at eight different concentrations.

Acknowledgements

We thank Robert Jäger, Bettina Hofmann, and Li-Hsing Wang for their excellent technical support during the computational studies. We thank Irwin Winkler, Jean-Paul Nicolas, and Alan Binnie for the experimental testing in the biogenic amine antitarget binding assay panel. Last but not least, we are thankful to Karl-Heinz Baringhaus for several helpful discussions and for critical reading of the manuscript.

Keywords: amines · drug design · G protein-coupled receptors · pharmacophore modeling · structure–activity relationships

[1] T. Klabunde, G. Hessler, *ChemBioChem* **2002**, *3*, 928 – 944.
[2] J. H. Kehne, B. M. Baron, A. A. Carr, S. F. Chaney, J. Elands, D. J. Feldman, R. A. Frank, P. L. van Giersbergen, T. C. McCloskey, M. P. Johnson, D. R. McCarty, M. Poirot, Y. Senyah, B. W. Siegel, C. Widmaier, *J. Pharmacol. Exp. Ther.* **1996**, *277*, 968 – 981.
[3] S. J. Peroutka, D. C. U'Prichard, D. A. Greenberg, S. H. Snyder, *Neuropharmacology* **1977**, *16*, 549 – 556.
[4] Aureus Pharma: www.aureus-pharma.com.
[5] E. Jacoby, A. Schuffenhauer, P. Floersheim, *Drug News Perspect.* **2003**, *16*, 93 – 102.
[6] Catalyst, Version 4.7, Accelrys Inc., San Diego, CA, **2002**.
[7] R. Barbaro, L. Betti, M. Botta, F. Corelli, G. Giannaccini, L. Maccari, F. Manetti, G. Strappaghetti, S. Corsano, *J. Med. Chem.* **2001**, *44*, 2118 – 2132.
[8] J. B. Bremner, R. Griffith, B. Coban, *Curr. Med. Chem.* **2001**, *8*, 607 – 620.
[9] MDL Information Systems Inc.: www.mdli.com.
[10] A. Evers, T. Klabunde, *J. Med. Chem.* **2005**, *48*, 1088 – 1097
[11] J. J. Chambers, D. E. Nichols, *J. Comput.-Aided Mol. Des.* **2002**, *16*, 511 – 520.
[12] J. Hwa, R. M. Graham, D. M. Perez, *J. Biol. Chem.* **1995**, *270*, 23 189 – 23 195.
[13] M. Ishiguro, *ChemBioChem* **2004**, *5*, 1210.
[14] N. J. Pollock, A. M. Manelli, C. W. Hutchins, M. E. Steffey, R. G. MacKenzie, D. E. Frail, *J. Biol. Chem.* **1992**, *267*, 17 780 – 17 786.
[15] L. Shi, J. A. Javitch, *Annu. Rev. Pharmacol. Toxicol.* **2002**, *42*, 437 – 467.
[16] N. Hamaguchi, T. A. True, D. L. Saussy, Jr., P. W. Jeffs, *Biochemistry* **1996**, *35*, 14 312 – 14 317.
[17] N. Hamaguchi, T. A. True, A. S. Goetz, M. J. Stouffer, T. P. Lybrand, P. W. Jeffs, *Biochemistry* **1998**, *37*, 5730 – 5737.
[18] R. B. Westkaemper, E. G. Hyde, M. S. Choudhary, N. Khan, E. I. Gelbar, R. A. Glennon, B. L. Roth, *Eur. J. Med. Chem.* **1999**, *34*, 441 – 447.
[19] D. A. Shapiro, K. Kristiansen, W. K. Kroeze, B. L. Roth, *Mol. Pharmacol.* **2000**, *58*, 877 – 886.
[20] SYBYL, Version 6.9, Tripos, Inc., St. Louis, MO, **2003**.
[21] D. W. Bonhaus, C. Bach, A. DeSouza, F. H. Salazar, B. D. Matsuoka, P. Zuppan, H. W. Chan, R. M. Eglen, *Br. J. Pharmacol.* **1995**, *115*, 622 – 628.
[22] D. K. Grandy, M. A. Marchionni, H. Makam, R. E. Stofko, M. Alfano, L. Frothingham, J. B. Fischer, K. J. Burke-Howie, J. R. Bunzow, A. C. Server, *Proc. Natl. Acad. Sci. USA* **1989**, *86*, 9762 – 9766.
[23] A. D. Michel, D. N. Loury, R. L. Whiting, *Br. J. Pharmacol.* **1989**, *98*, 883 – 889.
[24] D. Barlocco, G. Cignarella, V. D. Piaz, M. P. Giovannoni, P. G. De Benedetti, F. Fanelli, F. Montesano, E. Poggesi, A. Leonardi, *J. Med. Chem.* **2001**, *44*, 2403 – 2410.
[25] J. M. Wetzel, S. W. Miao, C. Forray, L. A. Borden, T. A. Branchek, C. Gluchowski, *J. Med. Chem.* **1995**, *38*, 1579 – 1581.
[26] R. Testa, L. Guarneri, E. Poggesi, P. Angelico, C. Velasco, M. Ibba, A. Cilia, G. Motta, C. Riva, A. Leonardi, *J. Pharmacol. Exp. Ther.* **1999**, *290*, 1258 – 1269.
[27] A. P. Ford, D. V. Daniels, D. J. Chang, J. R. Gever, J. R. Jasper, J. D. Lesnick, D. E. Clarke, *Br. J. Pharmacol.* **1997**, *121*, 1127 – 1135.
[28] W. Quaglia, M. Pigini, A. Piergentili, M. Giannella, G. Marucci, E. Poggesi, A. Leonardi, C. Melchiorre, *J. Med. Chem.* **1999**, *42*, 2961 – 2968.
[29] S. A. Buckner, K. W. Oheim, P. A. Morse, S. M. Knepper, A. A. Hancock, *Eur. J. Pharmacol.* **1996**, *297*, 241 – 248.
[30] T. G. Murali Dhar, D. Nagarathnam, M. R. Marzabadi, B. Lagu, W. C. Wong, G. Chiu, S. Tyagarajan, S. W. Miao, F. Zhang, W. Sun, D. Tian, Q. Shen, J. Zhang, J. M. Wetzel, C. Forray, R. S. Chang, T. P. Broten, T. W. Schorn, T. B. Chen, S. O'Malley, R. Ransom, K. Schneck, R. Bendesky, C. M. Harrell, K. P. Vyas, *J. Med. Chem.* **1999**, *42*, 4778 – 4793.

[31] D. Giardina, M. Crucianelli, R. Romanelli, A. Leonardi, E. Poggesi, C. Melchiorre, *J. Med. Chem.* **1996**, *39*, 4602 – 4607.
[32] M. A. Patane, R. M. DiPardo, R. P. Price, R. S. Chang, R. W. Ransom, S. S. O'Malley, J. Di Salvo, M. G. Bock, *Bioorg. Med. Chem. Lett.* **1998**, *8*, 2495 – 2500.
[33] B. A. Kenny, D. H. Chalmers, P. C. Philpott, A. M. Naylor, *Br. J. Pharmacol.* **1995**, *115*, 981 – 986.
[34] T. Wurch, C. Palmier, P. J. Pauwels, *Biochem. Pharmacol.* **2000**, *59*, 1117 – 1121.
[35] M. J. Millan, A. Gobert, A. Newman-Tancredi, F. Lejeune, D. Cussac, J. M. Rivet, V. Audinot, A. Adhumeau, M. Brocco, J. P. Nicolas, J. A. Boutin, N. Despaux, J. L. Peglion, *J. Pharmacol. Exp. Ther.* **2000**, *292*, 38 – 53.
[36] B. Baron, **2004**, personal communication.
[37] S. C. Sealfon, L. Chi, B. J. Ebersole, V. Rodic, D. Zhang, J. A. Ballesteros, H. Weinstein, *J. Biol. Chem.* **1995**, *270*, 16683 – 16688.
[38] S. P. Runyon, J. E. Savage, M. Taroua, B. L. Roth, R. A. Glennon, R. B. Westkaemper, *Bioorg. Med. Chem. Lett.* **2001**, *11*, 655 – 658.
[39] J. F. Vanhauwe, K. Josson, W. H. Luyten, A. J. Driessen, J. E. Leysen, *J. Pharmacol. Exp. Ther.* **2000**, *295*, 274 – 283.
[40] S. Patel, S. Freedman, K. L. Chapman, F. Emms, A. E. Fletcher, M. Knowles, R. Marwood, G. Mcallister, J. Myers, N. Curtis, J. J. Kulagowski, P. D. Leeson, M. Ridgill, M. Graham, S. Matheson, D. Rathbone, A. P. Watt, L. J. Bristow, N. M. Rupniak, E. Baskin, J. J. Lynch, C. I. Ragan, *J. Pharmacol. Exp. Ther.* **1997**, *283*, 636 – 647.
[41] C. Haubmann, H. Hubner, P. Gmeiner, *Bioorg. Med. Chem. Lett.* **1999**, *9*, 1969 – 1972.
[42] S. Okuyama, S. Chaki, R. Yoshikawa, Y. Suzuki, S. Ogawa, Y. Imagawa, N. Kawashima, Y. Ikeda, T. Kumagai, A. Nakazato, M. Nagamine, K. Tomisawa, *J. Pharmacol. Exp. Ther.* **1997**, *282*, 56 – 63.
[43] L. B. Kozell, K. A. Neve, *Mol. Pharmacol.* **1997**, *52*, 1137 – 1149.
[44] S. T. Phillips, T. de Paulis, B. M. Baron, B. W. Siegel, P. Seeman, H. H. Van Tol, H. C. Guan, H. E. Smith, *J. Med. Chem.* **1994**, *37*, 2686 – 2696.
[45] Y. Liao, B. J. Venhuis, N. Rodenhuis, W. Timmerman, H. Wikstrom, E. Meier, G. D. Bartoszyk, H. Bottcher, C. A. Seyfried, S. Sundell, *J. Med. Chem.* **1999**, *42*, 2235 – 2244.
[46] R. G. MacKenzie, D. VanLeeuwen, T. A. Pugsley, Y. H. Shih, S. Demattos, L. Tang, R. D. Todd, K. L. O'Malley, *Eur. J. Pharmacol.* **1994**, *266*, 79 – 85.

Received: October 14, 2004
Published online on March 24, 2005

